

Search for Lepton Flavour Violation in e^+e^- Collisions at $\sqrt{s} = 189 - 209$ GeV

The OPAL Collaboration

Abstract

We search for lepton flavour violating events ($e\mu$, $e\tau$ and $\mu\tau$) that could be directly produced in e^+e^- annihilations, using the full available data sample collected with the OPAL detector at centre-of-mass energies between 189 GeV and 209 GeV. In general, the Standard Model expectations describe the data well for all the channels and at each \sqrt{s} . A single $e\mu$ event is observed where according to our Monte Carlo simulations only 0.019 events are expected from Standard Model processes. We obtain the first limits on the cross-sections $\sigma(e^+e^- \rightarrow e\mu, e\tau$ and $\mu\tau)$ as a function of \sqrt{s} at LEP2 energies.

(Submitted to Physics Letters B)

The OPAL Collaboration

G. Abbiendi², C. Ainsley⁵, P.F. Åkesson³, G. Alexander²², J. Allison¹⁶, G. Anagnostou¹, K.J. Anderson⁹, S. Arcelli¹⁷, S. Asai²³, D. Axen²⁷, G. Azuelos^{18,a}, I. Bailey²⁶, E. Barberio⁸, R.J. Barlow¹⁶, R.J. Batley⁵, T. Behnke²⁵, K.W. Bell²⁰, P.J. Bell¹, G. Bella²², A. Bellerive⁹, S. Bethke³², O. Biebel³², I.J. Bloodworth¹, O. Boeriu¹⁰, P. Bock¹¹, J. Böhme²⁵, D. Bonacorsi², M. Boutemur³¹, S. Braibant⁸, L. Brigliadori², R.M. Brown²⁰, H.J. Burckhart⁸, J. Cammin³, R.K. Carnegie⁶, B. Caron²⁸, A.A. Carter¹³, J.R. Carter⁵, C.Y. Chang¹⁷, D.G. Charlton^{1,b}, P.E.L. Clarke¹⁵, E. Clay¹⁵, I. Cohen²², J. Couchman¹⁵, A. Csilling^{8,i}, M. Cuffiani², S. Dado²¹, G.M. Dallavalle², S. Dallison¹⁶, A. De Roeck⁸, E.A. De Wolf⁸, P. Dervan¹⁵, K. Desch²⁵, B. Dienes³⁰, M.S. Dixit^{6,a}, M. Donkers⁶, J. Dubbert³¹, E. Duchovni²⁴, G. Duckeck³¹, I.P. Duerdoth¹⁶, E. Etzion²², F. Fabbri², L. Feld¹⁰, P. Ferrari¹², F. Fiedler⁸, I. Fleck¹⁰, M. Ford⁵, A. Frey⁸, A. Fürties⁸, D.I. Futyan¹⁶, P. Gagnon¹², J.W. Gary⁴, G. Gaycken²⁵, C. Geich-Gimbel³, G. Giacomelli², P. Giacomelli², D. Glenzinski⁹, J. Goldberg²¹, K. Graham²⁶, E. Gross²⁴, J. Grunhaus²², M. Gruwé⁸, P.O. Günther³, A. Gupta⁹, C. Hajdu²⁹, M. Hamann²⁵, G.G. Hanson¹², K. Harder²⁵, A. Harel²¹, M. Harin-Dirac⁴, M. Hauschild⁸, J. Hauschildt²⁵, C.M. Hawkes¹, R. Hawkings⁸, R.J. Hemingway⁶, C. Hensel²⁵, G. Herten¹⁰, R.D. Heuer²⁵, J.C. Hill⁵, K. Hoffman⁹, R.J. Homer¹, D. Horváth^{29,c}, K.R. Hossain²⁸, R. Howard²⁷, P. Hüntemeyer²⁵, P. Igo-Kemenes¹¹, K. Ishii²³, A. Jawahery¹⁷, H. Jeremie¹⁸, C.R. Jones⁵, P. Jovanovic¹, T.R. Junk⁶, N. Kanaya²⁶, J. Kanzaki²³, G. Karapetian¹⁸, D. Karlen⁶, V. Kartvelishvili¹⁶, K. Kawagoe²³, T. Kawamoto²³, R.K. Keeler²⁶, R.G. Kellogg¹⁷, B.W. Kennedy²⁰, D.H. Kim¹⁹, K. Klein¹¹, A. Klier²⁴, S. Kluth³², T. Kobayashi²³, M. Kobel³, T.P. Kokott³, S. Komamiya²³, R.V. Kowalewski²⁶, T. Krämer²⁵, T. Kress⁴, P. Krieger⁶, J. von Krogh¹¹, D. Krop¹², T. Kuhl³, M. Kupper²⁴, P. Kyberd¹³, G.D. Lafferty¹⁶, H. Landsman²¹, D. Lanske¹⁴, I. Lawson²⁶, J.G. Layter⁴, A. Leins³¹, D. Lellouch²⁴, J. Letts¹², L. Levinson²⁴, J. Lillich¹⁰, C. Littlewood⁵, S.L. Lloyd¹³, F.K. Loebinger¹⁶, G.D. Long²⁶, M.J. Losty^{6,a}, J. Lu²⁷, J. Ludwig¹⁰, A. Macchiolo¹⁸, A. Macpherson^{28,l}, W. Mader³, S. Marcellini², T.E. Marchant¹⁶, A.J. Martin¹³, J.P. Martin¹⁸, G. Martinez¹⁷, G. Masetti², T. Mashimo²³, P. Mättig²⁴, W.J. McDonald²⁸, J. McKenna²⁷, T.J. McMahon¹, R.A. McPherson²⁶, F. Meijers⁸, P. Mendez-Lorenzo³¹, W. Menges²⁵, F.S. Merritt⁹, H. Mes^{6,a}, A. Michelini², S. Mihara²³, G. Mikenberg²⁴, D.J. Miller¹⁵, S. Moed²¹, W. Mohr¹⁰, T. Mori²³, A. Mutter¹⁰, K. Nagai¹³, I. Nakamura²³, H.A. Neal³³, R. Nisius⁸, S.W. O’Neale¹, A. Oh⁸, A. Okpara¹¹, M.J. Oreglia⁹, S. Orito²³, C. Pahl³², G. Pásztor^{8,i}, J.R. Pater¹⁶, G.N. Patrick²⁰, J.E. Pilcher⁹, J. Pinfold²⁸, D.E. Plane⁸, B. Poli², J. Polok⁸, O. Pooth⁸, A. Quadt³, K. Rabbertz⁸, C. Rembser⁸, P. Renkel²⁴, H. Rick⁴, N. Rodning²⁸, J.M. Roney²⁶, S. Rosati³, K. Roscoe¹⁶, Y. Rozen²¹, K. Runge¹⁰, D.R. Rust¹², K. Sachs⁶, T. Saeki²³, O. Sahr³¹, E.K.G. Sarkisyan^{8,m}, C. Sbarra²⁶, A.D. Schaile³¹, O. Schaile³¹, P. Scharff-Hansen⁸, M. Schröder⁸, M. Schumacher²⁵, C. Schwick⁸, W.G. Scott²⁰, R. Seuster^{14,g}, T.G. Shears^{8,j}, B.C. Shen⁴, C.H. Shepherd-Themistocleous⁵, P. Sherwood¹⁵, A. Skuja¹⁷, A.M. Smith⁸, G.A. Snow¹⁷, R. Sobie²⁶, S. Söldner-Rembold^{10,e}, S. Spagnolo²⁰, F. Spano⁹, M. Sproston²⁰, A. Stahl³, K. Stephens¹⁶, D. Strom¹⁹, R. Ströhmer³¹, L. Stumpf²⁶, B. Surrow²⁵, S. Tarem²¹, M. Tasevsky⁸, R.J. Taylor¹⁵, R. Teuscher⁹, J. Thomas¹⁵, M.A. Thomson⁵, E. Torrence¹⁹, D. Toya²³, T. Trefzger³¹, A. Tricoli², I. Trigger⁸, Z. Trócsányi^{30,f}, E. Tsur²², M.F. Turner-Watson¹, I. Ueda²³, B. Ujvári^{30,f}, B. Vachon²⁶, C.F. Vollmer³¹, P. Vannerem¹⁰, M. Verzocchi¹⁷, H. Voss⁸, J. Vossebeld⁸, D. Waller⁶, C.P. Ward⁵, D.R. Ward⁵,

P.M. Watkins¹, A.T. Watson¹, N.K. Watson¹, P.S. Wells⁸, T. Wengler⁸, N. Wermes³,
D. Wetterling¹¹, G.W. Wilson¹⁶, J.A. Wilson¹, T.R. Wyatt¹⁶, S. Yamashita²³, V. Zacek¹⁸,
D. Zer-Zion^{8,k}

¹School of Physics and Astronomy, University of Birmingham, Birmingham B15 2TT, UK

²Dipartimento di Fisica dell' Università di Bologna and INFN, I-40126 Bologna, Italy

³Physikalisches Institut, Universität Bonn, D-53115 Bonn, Germany

⁴Department of Physics, University of California, Riverside CA 92521, USA

⁵Cavendish Laboratory, Cambridge CB3 0HE, UK

⁶Ottawa-Carleton Institute for Physics, Department of Physics, Carleton University, Ottawa, Ontario K1S 5B6, Canada

⁸CERN, European Organisation for Nuclear Research, CH-1211 Geneva 23, Switzerland

⁹Enrico Fermi Institute and Department of Physics, University of Chicago, Chicago IL 60637, USA

¹⁰Fakultät für Physik, Albert Ludwigs Universität, D-79104 Freiburg, Germany

¹¹Physikalisches Institut, Universität Heidelberg, D-69120 Heidelberg, Germany

¹²Indiana University, Department of Physics, Swain Hall West 117, Bloomington IN 47405, USA

¹³Queen Mary and Westfield College, University of London, London E1 4NS, UK

¹⁴Technische Hochschule Aachen, III Physikalisches Institut, Sommerfeldstrasse 26-28, D-52056 Aachen, Germany

¹⁵University College London, London WC1E 6BT, UK

¹⁶Department of Physics, Schuster Laboratory, The University, Manchester M13 9PL, UK

¹⁷Department of Physics, University of Maryland, College Park, MD 20742, USA

¹⁸Laboratoire de Physique Nucléaire, Université de Montréal, Montréal, Quebec H3C 3J7, Canada

¹⁹University of Oregon, Department of Physics, Eugene OR 97403, USA

²⁰CLRC Rutherford Appleton Laboratory, Chilton, Didcot, Oxfordshire OX11 0QX, UK

²¹Department of Physics, Technion-Israel Institute of Technology, Haifa 32000, Israel

²²Department of Physics and Astronomy, Tel Aviv University, Tel Aviv 69978, Israel

²³International Centre for Elementary Particle Physics and Department of Physics, University of Tokyo, Tokyo 113-0033, and Kobe University, Kobe 657-8501, Japan

²⁴Particle Physics Department, Weizmann Institute of Science, Rehovot 76100, Israel

²⁵Universität Hamburg/DESY, II Institut für Experimental Physik, Notkestrasse 85, D-22607 Hamburg, Germany

²⁶University of Victoria, Department of Physics, P O Box 3055, Victoria BC V8W 3P6, Canada

²⁷University of British Columbia, Department of Physics, Vancouver BC V6T 1Z1, Canada

²⁸University of Alberta, Department of Physics, Edmonton AB T6G 2J1, Canada

²⁹Research Institute for Particle and Nuclear Physics, H-1525 Budapest, P O Box 49, Hungary

³⁰Institute of Nuclear Research, H-4001 Debrecen, P O Box 51, Hungary

³¹Ludwigs-Maximilians-Universität München, Sektion Physik, Am Coulombwall 1, D-85748 Garching, Germany

³²Max-Planck-Institute für Physik, Föhring Ring 6, 80805 München, Germany

³³Yale University, Department of Physics, New Haven, CT 06520, USA

^a and at TRIUMF, Vancouver, Canada V6T 2A3

^b and Royal Society University Research Fellow

^c and Institute of Nuclear Research, Debrecen, Hungary

^e and Heisenberg Fellow

^f and Department of Experimental Physics, Lajos Kossuth University, Debrecen, Hungary

^g and MPI München

ⁱ and Research Institute for Particle and Nuclear Physics, Budapest, Hungary

^j now at University of Liverpool, Dept of Physics, Liverpool L69 3BX, UK

^k and University of California, Riverside, High Energy Physics Group, CA 92521, USA

^l and CERN, EP Div, 1211 Geneva 23

^m and Tel Aviv University, School of Physics and Astronomy, Tel Aviv 69978, Israel.

1 Introduction

Within the minimal Standard Model (SM), the fermion mass matrices and the mechanism of electroweak symmetry breaking remain unexplained. The conservation of lepton number separately for each generation has no strong theoretical basis. In addition, recent data [1] present evidence for neutrino oscillations which necessarily violate lepton-flavour symmetry. Beyond the SM, lepton flavour violation (LFV) can occur in many supersymmetric (SUSY) extensions. An example is the SO(10) SUSY GUT model [2] where both the left- and right-handed supersymmetric lepton partners induce LFV, but none of the existing models predicts a measurable effect at LEP2 energies. Experimentally, no evidence for direct LFV has been reported so far. Upper bounds for muon decays are $\text{BR}(\mu^- \rightarrow e^- \gamma) < 1.2 \times 10^{-11}$ and $\text{BR}(\mu^+ \rightarrow e^+ e^+ e^-) < 10^{-12}$ [3]. Searches for neutrinoless τ decays [4] such as $\tau^+ \rightarrow e^+ e^+ e^-$ and $\tau^+ \rightarrow \mu^+ \mu^+ \mu^-$ yield upper limits $\text{BR}(Z \rightarrow e\tau) < 5.4 \times 10^{-5}$ and $\text{BR}(Z \rightarrow \mu\tau) < 7.1 \times 10^{-5}$ at 90% confidence level (CL). Direct searches in e^+e^- annihilations at the Z peak performed by the LEP experiments [5] yielded 95% CL limits $\text{BR}(Z \rightarrow e\mu, e\tau, \mu\tau) < \mathcal{O}(1) \times 10^{-5}$. In this paper we search for the $e\mu$, $e\tau$ and $\mu\tau$ final states in e^+e^- collisions at centre-of-mass energies between 189 GeV and 209 GeV.

2 Data sample and event simulation

The OPAL detector is described in detail in [6]. In the present analysis, the silicon micro vertex detector, the central tracking chambers, the electromagnetic calorimeter, the hadron calorimeter and the muon chambers were required to be fully operational. The full data sample collected since 1998 at $\sqrt{s} = 189$ GeV and above is analysed. The corresponding collected integrated luminosities are shown in Table 1.

Track reconstruction is performed by combining the information from the silicon micro vertex detector, the vertex drift chamber, the large volume jet drift chamber

and an outer layer of drift chambers for the measurement of the z coordinate¹ The OPAL electromagnetic calorimeter (ECAL) consists of a barrel part covering the region $|\cos\theta| < 0.82$ and two endcaps covering the region $0.82 < |\cos\theta| < 0.98$. A set of forward detectors provide complementary coverage for $\theta > 25$ mrad.

Detector acceptance and reconstruction efficiencies for processes under study are evaluated with two different methods based on Monte Carlo simulations. They are cross-checked with a third method that uses data only, where possible. The first method consists of generating $e\mu$, $e\tau$ and $\mu\tau$ signal events with the EXOTIC [7] generator using isotropic angular distributions. The second method uses Standard Model lepton pair final state events. The lepton pairs were simulated using `kk2f` [9] and `KORALZ` [10] for $\tau\tau(\gamma)$ and $\mu\mu(\gamma)$ and using `BHWIDE` [11] and `TEEGG` [12] for $ee(\gamma)$. Events passing the preselection are mixed to obtain $e\mu$, $e\tau$ and $\mu\tau$ topologies. The mixing assumes a uniform detector response in ϕ , and events are mixed only if the polar angles of their thrust axes are within 2 degrees of each other. The mixing is performed by rotating the momentum components in the plane transverse to the beam axis of a lepton from one event to match the lepton replaced in the mixed event. For each channel, the efficiency is estimated in bins of $\cos\theta$ and then averaged giving the same weight to each bin, in order to obtain a value that corresponds to a uniform angular distribution of the particles in the final state. The third method is the same as the second method but it uses a high purity sample of lepton pair events from the real data. The efficiencies after the final event selection (described in the next section) are almost independent of the centre-of-mass energy. They are shown in Table 1, after averaging for different centre-of-mass energies, together with their statistical and systematic uncertainties added in quadrature.

The SM background contributions are evaluated with large samples of events processed through a full simulation of the OPAL detector [8] and analysed using the same reconstruction and selection programs as applied to the data. The SM sample comprises lepton pair final states with initial and final state radiation, $q\bar{q}(\gamma)$ events generated with `PYTHIA` [13], a full set of four-fermion final states generated with `grc4f` [14] and `KORALW` [15] and gamma-gamma scattering events generated using `HERWIG` [16] and `PHOJET` [17]. SM Monte Carlo processes were generated at $\sqrt{s} = 189$ GeV, 192 GeV, 196 GeV and in steps of 2 GeV from 200 GeV to 208 GeV. The total generated SM sample corresponds to more than 500 times the integrated luminosity of the recorded data for $\tau^+\tau^-$, $\mu^+\mu^-$, $q\bar{q}$ and 4-fermion final states and to about 50 times the integrated luminosity of the recorded data for e^+e^- final states.

3 Event selection

Events with at least two and at most 8 measured tracks and no isolated photons in the electromagnetic calorimeters are considered for the analysis. Isolated photons

¹The OPAL coordinate system is defined so that the z axis is in the direction of the electron beam, the x axis points towards the centre of the LEP ring, and θ and ϕ are the polar and azimuthal angles, defined relative to the $+z$ - and $+x$ -axes, respectively. In cylindrical polar coordinates, the radial coordinate is denoted r .

are defined as in [18]. Each track should be consistent with originating from the interaction point with a measured momentum, P_{trk} , exceeding 250 MeV. An energy flow algorithm [19, 20] is used to measure each track and cluster energy, and to correct for possible double counting. The cone jet finder [21], with a cone half angle of 15° and a minimum cone energy of 10% of the beam energy, E_{beam} , is used and 2 jets are required in each event. Here, a single isolated track can form a jet if it has more energy than the minimum required energy in the cone. To gain in the energy resolution and remove potential background, namely Bhabha and gamma-gamma scattering, the momentum vector of each jet must satisfy $|\cos\theta| \leq 0.82$.

All three search channels have in common the feature that one of the event hemispheres should consist of a single electron or a single muon with a measured momentum close to E_{beam} . Events are selected for further analysis if:

- The total measured energy outside the two cones defining the jets is smaller than $0.10 \times E_{\text{beam}}$, the sum of the two jet energies is larger than E_{beam} and the event thrust is greater than 0.95. To have sensitivity to events produced at effective centre-of-mass energies lower than the actual \sqrt{s} , we accept events for which the total measured energy in both ends of the forward detectors is up to 10 GeV.
- One of the two jets has its energy greater than $0.8 \times E_{\text{beam}}$. That jet should contain a single isolated track, defined as a track with a momentum greater than $0.5 \times E_{\text{beam}}$ located in a cone with a 10° half opening angle. The 15° cone should not contain any other track that has a momentum in excess of $0.03 \times E_{\text{beam}}$.

After these cuts most of the hadronic final states and the $\gamma\gamma$ scattering events are rejected and the remaining event sample consists of 92% wide-angle Bhabha scattering events and $\simeq 8\%$ $\mu^+\mu^-$ and $\tau^+\tau^-$ events. The distributions of the visible energy (defined as the sum of all measured track energies), the total measured energy in the electromagnetic calorimeter and the $\cos\theta$ of the total momentum are shown in Figure 1. Here, the total momentum is defined as the vector sum of all measured momenta. The SM expectation describes the measured data well.

A track is considered to be the electron candidate if it has an associated energy in the electromagnetic calorimeter, E_{ECAL} , within 20% of E_{beam} and if the ratio $E_{\text{ECAL}}/P_{\text{trk}}$ is greater than 0.7. The track should also have a characteristic ionisation in the tracking chambers consistent with an electron hypothesis. A track is considered to be a muon candidate if it has matching hadron calorimeter and muon chamber hits and if the ratio $E_{\text{ECAL}}/P_{\text{trk}}$ is less than 0.1. The following cuts, common to all three search channels, are applied:

1. To reject the Bhabha scattering, events are selected if the total measured energy in the electromagnetic calorimeter is less than $1.6 \times E_{\text{beam}}$.

OPAL

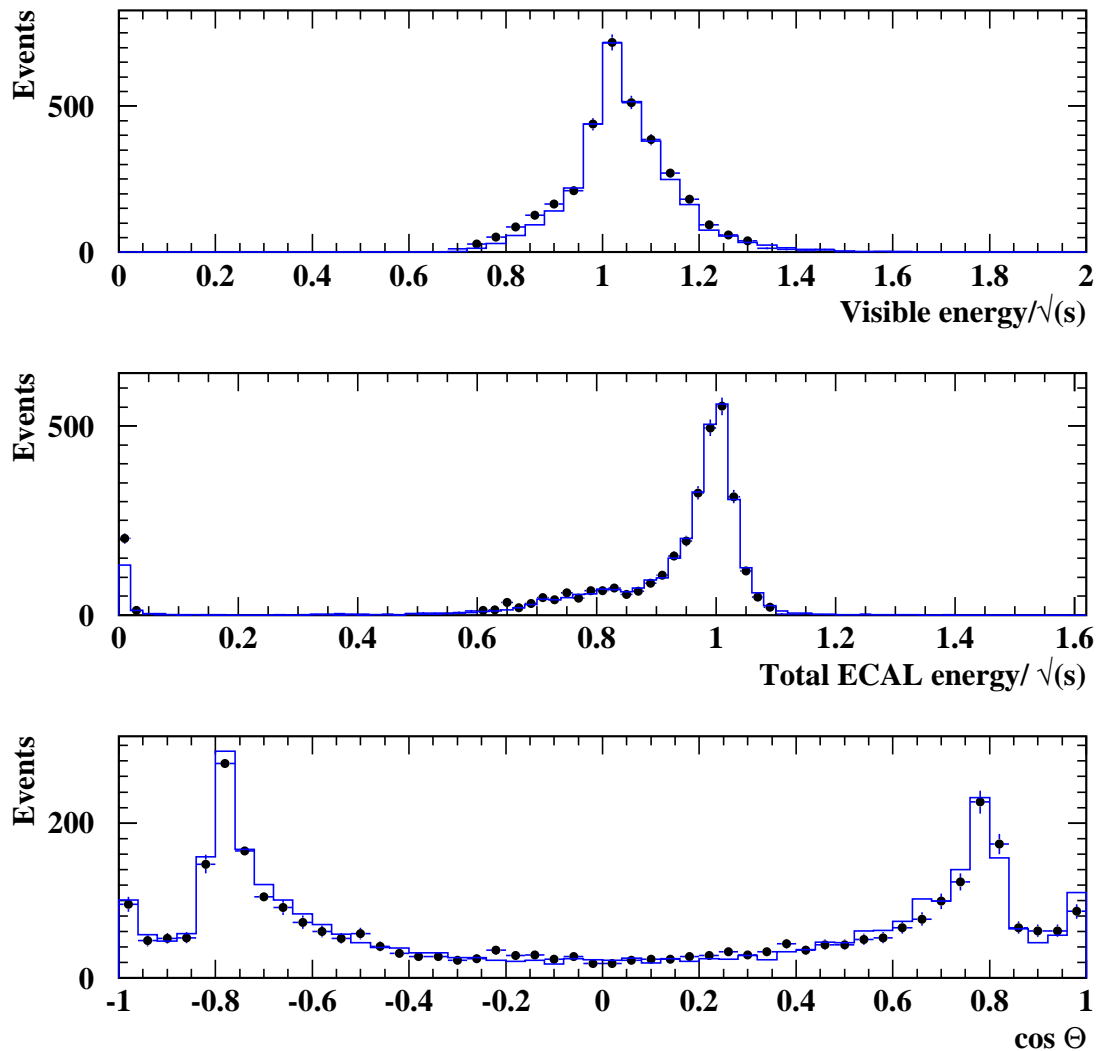


Figure 1: The measured visible energy, the total measured energy in the electromagnetic calorimeter and the $\cos \theta$ of the total momentum for all data (points) as compared to the Standard Model Monte Carlo expectation (solid lines). The small asymmetry in the total momentum distribution is caused by the fact that the interaction vertex is not the geometrical center of the OPAL detector. They are about $\simeq 1$ cm away from each other. But this effect is well modelled in the Monte Carlo.

2. Events that have a reconstructed electron candidate in the transition region between the barrel and endcaps ($0.75 < |\cos\theta| < 0.85$) are rejected, ensuring that the remaining electron candidates have a good energy resolution.
3. To reduce the e^+e^- and $\mu^+\mu^-$ background further, events that have two muon or two electron candidates are rejected. This reduces the $e\tau$ and $\mu\tau$ efficiencies by about 15% each, rejecting events with $\tau \rightarrow \nu\bar{\nu}e$ or $\nu\bar{\nu}\mu$ where the final state electron or muon satisfies the requirement of an isolated track associated with an electron or a muon.
4. To suppress the $\tau^+\tau^-$ final states, events with two isolated tracks are rejected if each track has a measured momentum less than $0.30 \times E_{\text{beam}}$. They are also rejected if the opening angle between the two isolated tracks is less than 160 degrees.

The distribution of $E_{\text{ECAL}}/E_{\text{beam}}$ for electron candidates and the distribution of $P_{\text{trk}}/E_{\text{beam}}$ for muon candidates are shown in Figure 2. These distributions are obtained for the selected events after cut 1 above and show good agreement between data and SM expectations. Using Monte Carlo lepton pair final states, we find that the resolution on E_{ECAL} is 3.5% for electrons and the resolution on P_{trk} is 11% for muons.

Events that survive the above cuts are subject to specific $e\mu$, $e\tau$ and $\mu\tau$ selection cuts. These cuts are optimised to minimise the dependence on \sqrt{s} and to reject SM lepton pair final states while keeping reasonable efficiency for $e\mu$, $e\tau$ and $\mu\tau$.

- **Selection for the $e\mu$ channel:** The event is required to have only two isolated tracks with opposite charge where each of the tracks belongs to a different jet. One of the tracks should be identified as an electron and its measured energy should be within 15% of the beam energy. The second track should be identified as a muon candidate with a measured momentum within 20% of the beam energy. The total event momentum is required to be less than $0.25 \times E_{\text{beam}}$. In the case where the opening angle between the two tracks is less than 170° , we require in addition that the missing momentum should be pointing to the forward part of the detector ($|\cos\theta| > 0.9$). Missing momentum caused by undetected neutrinos from a τ decay would, for the selected events, point to the barrel part of the detector.
- **Selection for the $e\tau$ channel:** Here we apply tighter cuts on the electron candidate. The electron should be identified as an isolated track with $|E_{\text{ECAL}} - E_{\text{beam}}|/E_{\text{beam}} < 0.10$. The energy of the recoiling jet against the electron is required to be less than $0.75 \times E_{\text{beam}}$, and the total event momentum should be larger than 5 GeV and point to the barrel region of the detector.
- **Selection for the $\mu\tau$ channel:** Here we require an identified muon as an isolated track with $|P_{\text{trk}} - E_{\text{beam}}|/E_{\text{beam}} < 0.15$. The energy of the jet recoiling against the muon is required to be less than $0.75 \times E_{\text{beam}}$, and the total event momentum should be larger than 5 GeV and point to the barrel region of the detector.

OPAL

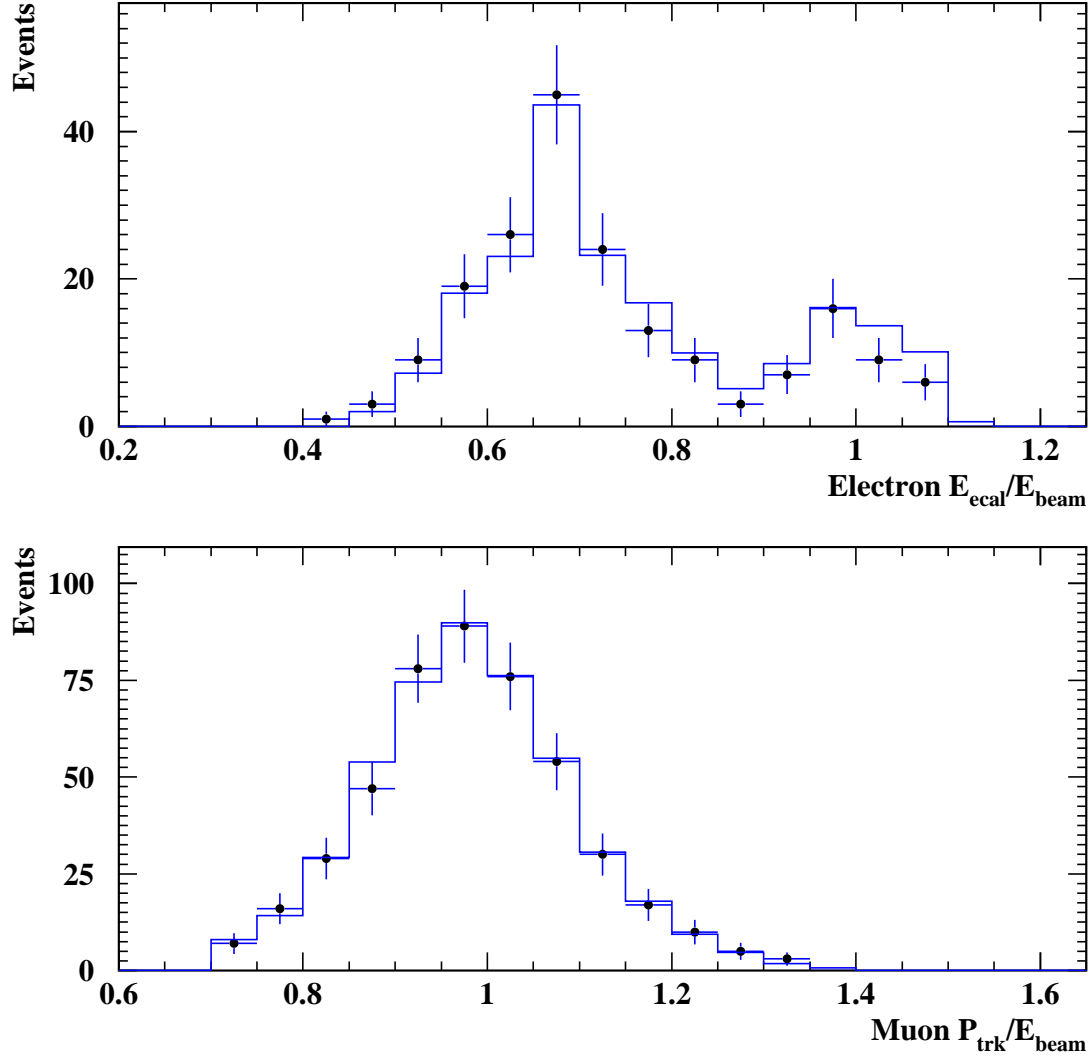


Figure 2: The E_{ECAL}/E_{beam} distribution for electron candidates and the P_{trk}/E_{beam} for muon candidates for all data (points) as compared to the Standard Model Monte Carlo expectation (solid lines).

Table 1: Integrated luminosity and efficiency as a function of \sqrt{s} .

| \sqrt{s} (GeV) | Lumi. [pb^{-1}] | $e\mu$ [%] | $e\tau$ [%] | $\mu\tau$ [%] |
|------------------------------|----------------------------|----------------|----------------|----------------|
| 189 | 174.6 | 56.3 ± 0.7 | 24.6 ± 0.5 | 22.2 ± 0.6 |
| $192 < \sqrt{s} < 200$ | 103.6 | 56.0 ± 0.7 | 24.2 ± 0.5 | 21.8 ± 0.6 |
| $200 \leq \sqrt{s} \leq 209$ | 322.2 | 55.8 ± 0.7 | 23.9 ± 0.5 | 21.8 ± 0.6 |

Table 2: Selected data events versus SM expectations. “No- $\ell^+\ell^-$ ” stands for the cut against events having a pair of electron (e^+e^-) or a pair of muon ($\mu^+\mu^-$) candidates in the final state.

| | e^+e^- | $\mu^+\mu^-$ | $\tau^+\tau^-$ | Other | Total Background | Data |
|--|----------|--------------|----------------|-------|------------------|-------|
| Selected | 20745 | 1359 | 564 | 24 | 22683 | 23164 |
| $\sum E_{\text{ECAL}} < 1.6 E_{\text{beam}}$ | 2275 | 1359 | 520 | 23 | 4185 | 4201 |
| No- $\ell^+\ell^-$ | 559 | 57 | 67 | 21 | 704 | 713 |
| $e\mu$ Candidates | 0 | 0 | 0.015 | 0.004 | 0.019 | 1 |
| $e\tau$ Candidates | 4.010 | 0.017 | 0.520 | 0.004 | 5.01 | 5 |
| $\mu\tau$ Candidates | 0.017 | 5.901 | 8.400 | 0 | 14.3 | 11 |

With our lepton identification criteria, a hadron from a single-prong tau decay has a 3% probability to be misidentified as an electron and a 1.6% probability to be misidentified as muon.

4 Results

After the normalisation of the Monte Carlo backgrounds to the integrated luminosity of the data, the effects of the selection criteria are summarised in Table 2. The contributions to the SM background from processes other than lepton pair final states (e^+e^- , $\mu^+\mu^-$ and $\tau^+\tau^-$) are very small. These contributions include the full 4-fermion final states, QCD-like final states and $\gamma\gamma$ scattering events. They are summed together in the table as a separate column.

The SM describes the data well for each \sqrt{s} and each step of the selection procedure, except for a single $e\mu$ candidate which was selected at $\sqrt{s} = 189$ GeV. According to our Monte Carlo simulations only 0.019 events are expected from SM processes. This particular event is displayed in Figure 3 for the $r - \phi$ view and in Figure 4 for the $r - \theta$ view. It has the following characteristics:

- total visible energy $E_{\text{vis}} = 176$ GeV ($\sqrt{s} = 189$ GeV);
- measured ECAL energy of the electron candidate: $E_{\text{ECAL}} = (84.83 \pm 2.25)$ GeV;
- measured momentum of the muon candidate: (84.5 ± 10) GeV;

Table 3: 95% confidence level upper limits on $\sigma(e^+e^- \rightarrow e\mu, e\tau \text{ and } \mu\tau)$ as a function of \sqrt{s} .

| Channel | $e\mu$ | $e\tau$ | $\mu\tau$ |
|------------------------------|---------------------|---------------------|---------------------|
| $\sqrt{s}(\text{GeV})$ | $\sigma[\text{fb}]$ | $\sigma[\text{fb}]$ | $\sigma[\text{fb}]$ |
| 189 | 58 | 95 | 115 |
| $192 \leq \sqrt{s} \leq 196$ | 62 | 144 | 116 |
| $200 \leq \sqrt{s} \leq 209$ | 22 | 78 | 64 |

- opening angle between the two tracks = 165° ;
- one measured cluster in the forward detector with $E = 7.2 \pm 2.5$ GeV.

A kinematic fit with energy-momentum conservation is applied assuming that the forward detector cluster was due to a photon. The fit has a probability of 41%.

Results of the present search are quantified in terms of 95% CL upper limits of the production cross section of LFV events, assuming uniform final state angular distributions. The upper limits are obtained with the method that takes into account the uncertainties on the signal efficiency and on the background expectation as explained in Reference [22]. These uncertainties include systematic contributions discussed in the next section. The upper limits are displayed in Table 3 for different intervals of \sqrt{s} . Limits for different assumed angular distributions may be derived using the fact that the efficiency is uniform over the barrel region of the detector.

5 Systematic Studies

Five inputs are used to estimate the upper limits: the number of selected event candidates, the SM background contribution, the signal selection efficiency and the uncertainties on the background expectation and on the signal efficiency. These uncertainties are estimated by repeating the analysis while varying the applied cuts, taking into account the following effects:

- **Efficiency:** The two Monte Carlo methods (see Section 2) yield compatible results. The data-based method is applied only to the $e\mu$ channel, since at each \sqrt{s} , the reconstructed $\tau^+\tau^-$ sample is too small to apply the method. A systematic error of 1% for $e\mu$ and of 2.1% for $e\tau$ and $\mu\tau$ is assigned based on the largest deviation between the methods.
- **Event selection:** The following variations in the event selections are made, one at a time: the maximum number of allowed tracks per event is changed from 8 to 10; the minimum track momentum is increased from 250 to 500 MeV; the cone angle is opened from 15° to 30° ; the cone minimum energy is increased from 10% to 20% of E_{beam} ; the cut on the event thrust is set to 0.98 instead of 0.95.

- **Energy and momentum resolution:** The electromagnetic calorimeter energy resolution is about 3.5% for electrons with momenta above 70 GeV. The systematic error is estimated by scaling the measured electromagnetic energy of electron candidates by $\pm 3.5\%$. The measured momenta of muon candidates are varied by $\pm 10\%$ to account for the momentum resolution.
- **Integrated luminosity:** A 0.5% measurement error on the integrated luminosity is added to another 0.5% interpolation and averaging error between various grouped \sqrt{s} points (see Table 1), after which the corresponding error on the SM contribution is calculated.

The different errors are added in quadrature. The final systematic uncertainty is about 3.5% on the efficiency and 5% on the background expectation.

6 Conclusion

We have no clear evidence for production of lepton flavour violating events such as $e\mu$, $e\tau$ and $\mu\tau$ production in e^+e^- collisions between 189 GeV and 209 GeV. We observe one single $e\mu$ candidate, probably produced with initial state radiation, where, according to our Monte Carlo simulations, we expect 0.019 events to be produced from Standard Model processes. We have obtained the first upper limits for $\sigma(e^+e^- \rightarrow e\mu, e\tau \text{ and } \mu\tau)$ as a function of \sqrt{s} at LEP2 energies. The limits range from 22 fb to 58 fb for the $e\mu$ channel, from 78 fb to 144 fb for the $e\tau$ channel and from 64 fb to 166 fb for the $\mu\tau$ channel.

Acknowledgements:

We particularly wish to thank the SL Division for the efficient operation of the LEP accelerator at all energies and for their continuing close cooperation with our experimental group. We thank our colleagues from CEA, DAPNIA/SPP, CE-Saclay for their efforts over the years on the time-of-flight and trigger systems which we continue to use. In addition to the support staff at our own institutions we are pleased to acknowledge the

Department of Energy, USA,

National Science Foundation, USA,

Particle Physics and Astronomy Research Council, UK,

Natural Sciences and Engineering Research Council, Canada,

Israel Science Foundation, administered by the Israel Academy of Science and Humanities,

Minerva Gesellschaft,

Benozio Center for High Energy Physics,

Japanese Ministry of Education, Science and Culture (the Monbusho) and a grant under the Monbusho International Science Research Program,

Japanese Society for the Promotion of Science (JSPS),
German Israeli Bi-national Science Foundation (GIF),
Bundesministerium für Bildung und Forschung, Germany,
National Research Council of Canada,
Research Corporation, USA,
Hungarian Foundation for Scientific Research, OTKA T-029328, T023793 and OTKA
F-023259.

References

- [1] Y. Fukuda et al., Super-Kamiokande Collaboration, Phys. Lett. B433, (1998) 9;
Phys. Lett. B436, (1998) 33; Phys. Rev. Lett. 81, (1998) 1562;
T. Ishii, hep-ex/0106008;
J.N. Bahcall et al., Nucl. Phys. Proc. Suppl. 100 (2001) 5.
“Measurement of the rate of $\nu_e + d \rightarrow p + p + e^-$ interactions produced by
 ^8B solar neutrinos at the Sudbury Neutrino Observatory”, SNO Collaboration,
nucl-ex/0106015, submitted to Phys. Rev. Lett.
- [2] R. Barbieri, L. Hall and A. Strumi, Nucl. Phys. B445, (1995) 219;
Y. Okada, “Susy Phenomenology”, KEK-TH-606, hep-ph/9811502.
- [3] D.E. Groom et al., Eur. Phys. J. C15 (2000) 1.
- [4] Argus Collaboration. H. Albrecht et al., Z. Phys. C55 (1992) 179;
CLEO Collaboration, T. Bowcock et al., Phys. Rev. D41 (1990) 805.
- [5] OPAL Collaboration, M.Z. Akrawy et al., Phys. Lett. B254 (1991) 293;
ALEPH Collaboration, D. Decamp et al., Phys. Rep. 216 (1992) 253;
DELPHI Collaboration, P. Abreu et al., Phys. Lett. B298 (1992) 247;
L3 Collaboration, O. Adriani et al., Phys. Lett. B316 (1993) 427.
- [6] OPAL Collaboration, K. Ahmet et al., Nucl. Inst. Meth. A305 (1991) 275;
S. Anderson et al., Nucl. Instr. Meth. A403 (1998) 326;
B.E. Anderson et al., IEEE Trans. on Nucl. Science 41 (1994) 845;
G. Aguillon et al., Nucl. Instr. Meth. A416 (1998) 266.
- [7] A. Djouadi, Z. Phys. C63 (1994) 317;
F. Boudjema, A. Djouadi and J.L. Kneur, Z. Phys. C57 (1993) 425;
R. Tafirout and G. Azuelos, Comp. Phys. Comm. 126 (2000) 244.
- [8] J. Allison et al., Nucl. Instr. Meth. A317 (1992) 47.
- [9] S. Jadach, B.F.L. Ward and Z. Was, Phys. Lett. B449 (1999) 97.
- [10] S. Jadach, W. Placzek and B.F.L. Ward and Z. Was, Comp. Phys. Comm. 79
(1994) 503.
- [11] S. Jadach, W. Placzek and B.F.L. Ward, Phys. Lett. B390 (1997) 298.

- [12] D. Karlen, Nucl. Phys. B289 (1987) 23.
- [13] T. Sjöstrand, Comp. Phys. Comm. 82 (1994) 74.
- [14] J. Fujimoto et al., Comp. Phys. Comm. 100 (1997) 128.
- [15] S. Jadach et al., KORALW1.42, CERN-TH/98-242.
- [16] G. Marchesini et al., Comp. Phys. Comm. 67 (1992) 465.
- [17] R. Engel and J. Ranft, Phys. Rev. D54 (1996) 4244.
- [18] OPAL Collaboration K. Ackerstaff et al., Eur. Phys. J. C1 (1998) 31.
- [19] OPAL Collaboration, M.Z. Akrawy et al., Phys. Lett. B253 (1991) 511;
OPAL Collaboration, K. Ackerstaff et al., Phys. Lett. B389 (1996) 616.
- [20] OPAL Collaboration, K. Ackerstaff et al., Eur. Phys. J. C2 (1998) 213
- [21] UA1 Collaboration, G. Arnison et al., Phys. Lett. B122 (1983) 103;
J.E. Huth et al., Snowmass (1990) Ed. E.L. Berger, World Scientific, Singapore
(1990) 134;
OPAL Collaboration, R. Akers et al., Z. Phys. C63 (1994) 197.
- [22] T. Junk, Nucl. Inst. Meth. A434 (1999) 435.

```
Run:event 9298:115615   Ctrk(N= 2 Sump=168.4) Ecal(N= 4 SumE= 84.9)
Ebeam 94.32 Vtx ( -.04, .08, .44) Hcal(N= 4 SumE= 5.1) Muon(N= 1)
```

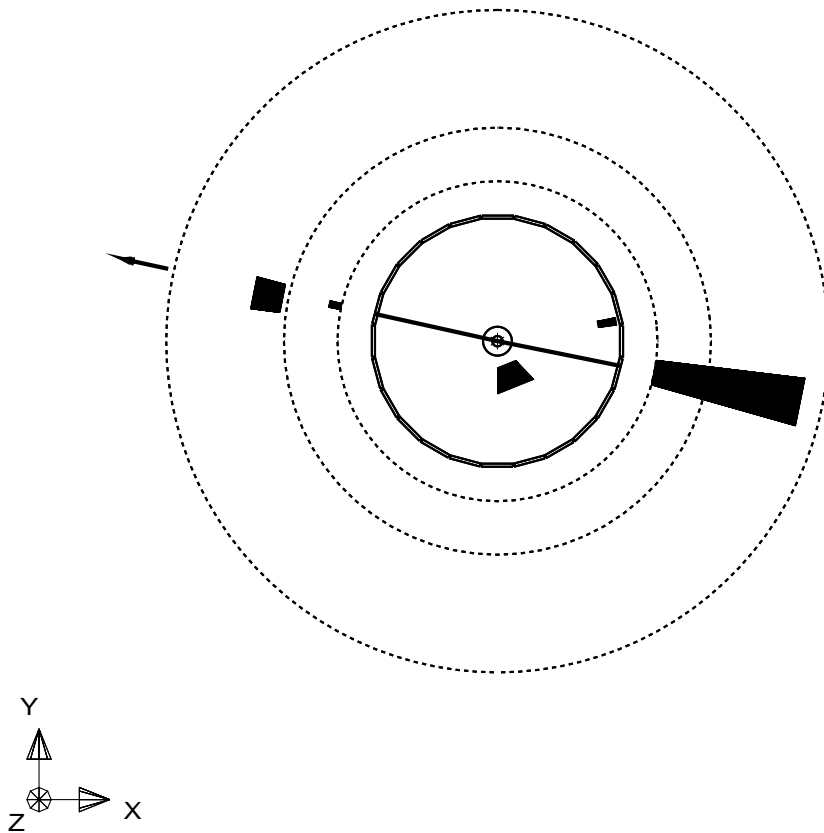


Figure 3: An $r - \phi$ view of the $e\mu$ candidate at 189 GeV. Two well measured tracks can be seen in the trackers (inner thick circle). The track in the right side deposited all its energy in the electromagnetic calorimeter (black trapezoid), and is the electron candidate. The track in the left side has a small electromagnetic energy deposit and has matching muon hits in the muon chambers (the arrow), and is the muon candidate.

```

Run:event 9298:115615   Ctrk(N= 2 Sump=168.4) Ecal(N= 4 SumE= 84.9)
Ebeam 94.32 Vtx ( -.04, .08, .44) Hcal(N= 4 SumE= 5.1) Muon(N= 1)

```

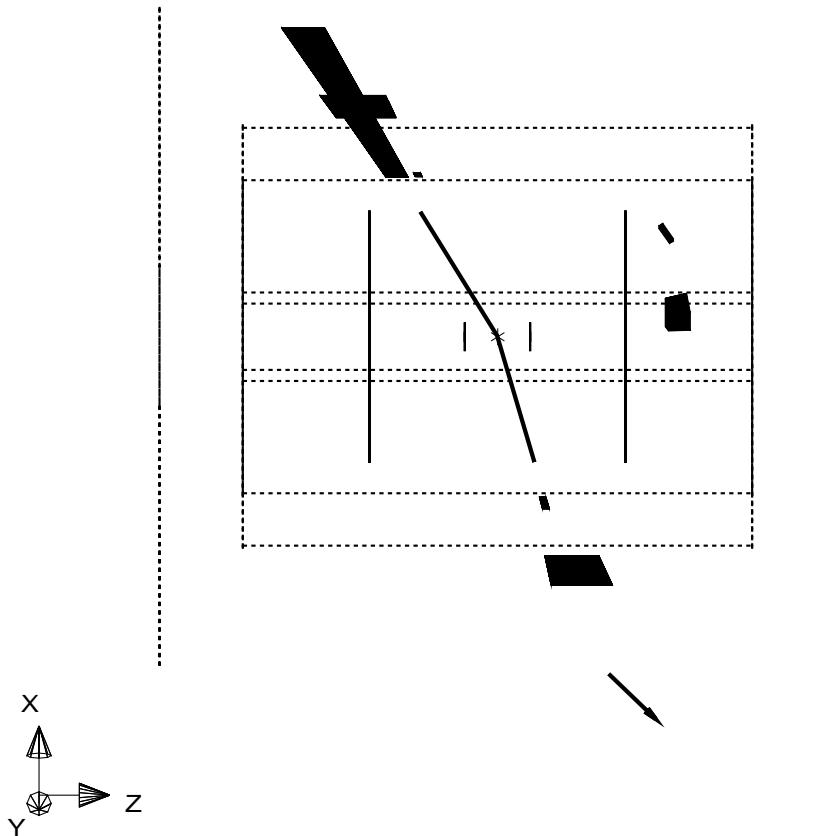


Figure 4: An $r - \theta$ view of the $e\mu$ candidate at 189 GeV. The beam direction is a horizontal line passing through the intersection of the two tracks. The tracks are not back-to-back, and the missing momentum is compatible with the observed cluster in the forward detector which is the dark block close to the beam axis (right side).